Frontiers of Physics
https://doi.org/10.1007/s11467-019-0904-5
Front. Phys.
14(4), 43604 (2019)

RESEARCH ARTICLE

Computationally predicting spin semiconductors and half metals from doped phosphorene monolayers

Jing-Hua Feng (冯景华)[1,2], **Geng Li** (李庚)[2,†], **Xiang-Fei Meng** (孟祥飞)[2], **Xiao-Dong Jian** (菅晓东)[2], **Zhen-Hong Dai** (戴振宏)[3], **Yin-Chang Zhao** (赵银昌)[3], **Zhen Zhou** (周震)[4,‡]

[1] *College of Computer, National University of Defense Technology, Changsha 410073, China*
[2] *National Supercomputer Center in Tianjin, Tianjin 300457, China*
[3] *Department of Physics, Yantai University, Yantai 264005, China*
[4] *School of Materials Science and Engineering, Computational Centre for Molecular Science, Institute of New Energy Material Chemistry, Nankai University, Tianjin 300350, China*
Corresponding authors. E-mail: [†] *ligeng@nscc-tj.cn,* [‡] *zhouzhen@nankai.edu.cn*
Received April 24, 2019; accepted May 7, 2019

First-principles computations are performed to investigate phosphorene monolayers doped with 30 metal and nonmetal atoms. The binding energies indicate the stability of all doped configurations. Interestingly, the magnetic atom Co doping induces the absence of the magnetism while the magnetism is realized in phosphorene with substitutional doping of nonmagnetic atoms (O, S, Se, Si, Br, and Cl). The magnetic moment of transition metal (TM)-doped systems is suppressed in the range of 1.0-3.97 μ_B. The electronic properties of the doped systems are modulated differently; O, S, Se, Ni, and Ti doped systems become spin semiconductors, while V doping makes the system a half metal. These results demonstrate potential applications of functionalized phosphorene with external atoms, in particular to spintronics and dilute magnetic semiconductors.

Keywords phosphorene, spin semiconductors, half metals, density functional theory

1 Introduction

Since the discovery of grapehene in 2004, two-dimensional (2D) materials (such as graphene silicene, BN, and MoS_2) have attracted tremendous attention in exploring usual condensed-matter physical phenomena [1, 2] and are expected to play a significant role in nanoscale devices [3]. Development of field-effect transistors (FETs) requires candidates with both a reasonably high carrier mobility and a moderate electronic band gap. Massless Dirac fermions endow graphene with high carrier mobility, but its semimetallic characteristic makes it impossible in device applications [4, 5]. Although MoS_2 possesses a direct band gap of 1.88 eV [6], the charge carrier mobility of 200 $cm^2 \cdot V^{-1} \cdot s^{-1}$ is not enough for applications and it is also lack of efficient methods to modulate its n-type conductance and carrier concentration [5, 7], which are two obstacles for its extensive applications.

Black phosphorus (BP) is the most stable phosphorus allotrope at room temperature that was first synthesized from white phosphorus under high pressure and high temperature in 1914, and then its structure was confirmed by experiments accurately [8]. Research in the 1960s disclosed that BP combines high carrier mobility with a fundamental band gap, which becomes a most promising candidate material for post-silicon semiconductor applications [9]. Phosphorene, an atom-thick-layer BP sheet arranged in a 2D honeycomb lattice, is a new stable allotrope of phosphorus, similar to graphene and MoS_2. Recently, it has been successfully exfoliated from bulk BP [5, 10, 11], which consists of stacked puckered 2D honeycomb layers coupled together via interlayer weak van der Waals interactions [12]. The structural and physical properties of phosphorene have been extensively studied both experimentally [5, 10] and computationally [13, 14]. Inside the phosphorene layer, each P atom forms sp^3 hybridization with three neighboring P atoms, resulting in a puckered honeycomb structure [13, 14].

In monolayer BP, translational symmetry in the z direction is broken, and its band structure has a direct energy gap about 1.0 eV at the Γ point, which is much larger than that of bulk BP with the value about 0.31–0.36 eV [13, 15]. Phosphorene is a 2D p-type semiconductor complementary to n-type MoS_2. Moreover, phosphorene-based FETs have been fabricated and demonstrate good device performance with an extremely high hole mobility of 300–1000 $cm^2 \cdot V^{-1} \cdot s^{-1}$ and an I_{on}/I_{off} ratio of up to 10^4 at room temperature [5, 10, 11, 15]. As a result, 2D phosphorene possesses an intriguing application in future nanodevices.

Spintronic devices and dilute magnetic semiconductors are widely used in transforming information and design-

ing qubits for quantum computing, data storage, and coding or decoding, by taking advantage of different spin polarized electronic energy states in materials [22–27]. Half metals and spin semiconductors are two kinds of typical materials. Only one spin state in a half metal is conducting and the other spin state is insulating [23, 24]. Due to an energy gap between two different spin states in spin semiconductors, the carriers are fully spin polarized with either electrons conducting one spin or holes conducting the other one [23, 24].

It is a common way to create vacancies by high-energy atom/ion bombardment and fill these vacancies with desired dopants to realize half metal and spin-semiconducting properties [28, 29]. Many experiments and computations have been performed to find half metal and spin-semiconducting properties in 2D nanostructures, such as graphene, BN and its nanoribbons [23, 24, 29–32]. The effects made by the dopants on the monolayer phosphorene attract our interest.

In this work, we systematically investigated the structural, energetic, electronic, and magnetic properties of phosphorene doped by 30 different metal and non metal atoms from periods two, three, and four. The binding energies for all doped systems are larger than zero. The spin polarized semiconducting state is realized in phosphorene by substitutional doping of O, S, Se, Ni, and Ti, while a half-metallic state is obtained by V doping. The magnetic moments of transition metal (TM) doped phosphorene monolayers stem from the valence electrons of the TM $3d$ orbitals while the magnetic moments of the nonmetal atoms doping originate from the structural distortion.

2 Computational details

Our doped systems, as shown in Fig. 1(a), were simulated by using Vienna ab initio simulation package (VASP) code [33], which uses the plane wave basis and is based on the spin-polarized density functional theory (DFT). We adopted projector augmented-wave (PAW) potentials [34] to deal with the interaction between the ion cores and valence electrons with the kinetic energy cutoff of 400 eV. The valence electron exchange and correlation potentials are described by the generalized gradient approximation with the Perdew–Burke–Ernzerhof (PBE) functional [35]. A $3 \times 4 \times 1$ phosphorene supercell including 47 atoms and 1 doped atom is employed and the impurity concentration is 2.08%. The vacuum space along the periodic directions is larger than 15 Å to avoid any interaction between the slabs. The energy convergence criterion for electronic iteration is 10^{-5} eV. All the geometries and lattice parameters are fully optimized by using the conjugate gradient algorithm until the Hellmann–Feynman forces on each atom are less than 10 meV/Å. For a $3 \times 4 \times 1$ doped phos-

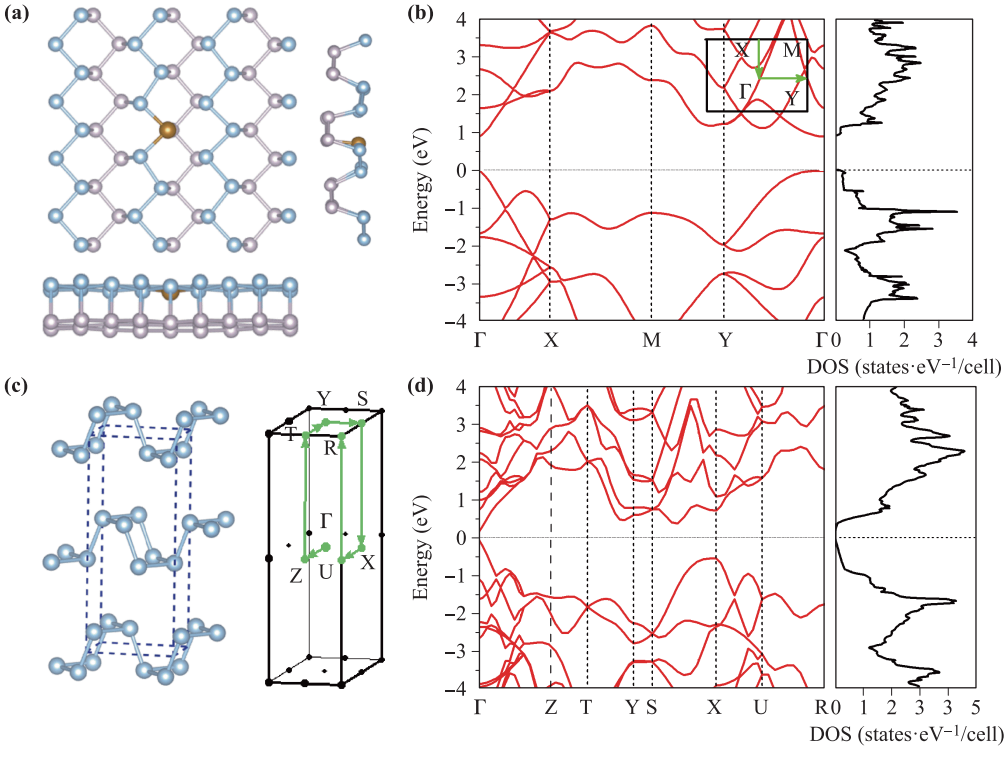

Fig. 1 **(a)** Top and side view of the 3×4 puckered hexagonal structure of monolayer phosphorene with one doped atom. **(b)** Electronic band structure (left) and DOS (right) for monolayer phosphorene with the inset of the associated Brillouin zone path. **(c)** Crystal structure and Brillouin zone path of bulk BP primitive cell. **(d)** Electronic band structure (left) and DOS (right) for bulk BP. The Fermi level is set to be zero.

phorene supercell, the Brillouin zone (BZ) is sampled by a Monkhorst–Pack [36] k-point mesh of $3 \times 3 \times 1$ for the structure optimizations, while a $9 \times 9 \times 1$ k-grid is adopted for static and density of state (DOS) calculations.

3 Results and discussion

3.1 Pristine monolayer phosphorene

Bulk BP is the graphite counterpart of phosphorene (Fig. 1(a)), where the phosphorene layers are held together through van der Waals interactions, as seen in Fig. 1(c). Our computed lattice constants for bulk BP are $a = 3.31$ Å, $b = 4.56$ Å and $c = 11.20$ Å, which are in good agreement with experimental and computational values [37]. Unlike the flat structure of graphene, monolayer phosphorene has four P atoms arranged in a puckered honeycomb lattice with each phosphorus atom forming sp^3 hybridization with three adjacent atoms, as shown in Fig. 1(a). The optimized lattice parameters for monolayer phosphorene are $a = 3.30$ Å and $b = 4.63$ Å, consistent with the previous computational results [38]. The electronic band structure and density of states (DOS) for phosphorene and bulk BP are presented in Figs. 1(b) and (d), respectively. Bulk BP is a direct semiconductor with a band gap of 0.12 eV. Phosphorene also has a direct band gap of 0.91 eV at the Γ point, which is close to the recently measured band gap of 1.0–1.5 eV for monolayer phosphorene in experiments [5, 39]. The conduction band minimum (CBM) and the valence band maximum (VBM) located at the Γ point are mainly contributed by p_z orbitals of the P atoms.

A hexagonal supercell consisting of the $3 \times 4 \times 1$ phosphorene unit cells with 13.37×13.74 Å^2 lateral dimensions is constructed for the doped system, as shown in Fig. 1(a). The distance of the neighboring doped atoms is about 13.0 Å and the doping concentration is approximately 2.08%. Thus the coupling interaction between the doped atoms is rather weak so that the doped phosphorene systems can be considered to be an approximation of the interaction between an isolated atom and the phosphorene. We define the binding energy of atoms doped in phosphorene as:

$$E_b(M) = E(M) + E(\text{Vacancy}) - E(\text{M-Phosphorene}), \quad (1)$$

where $E(M)$, $E(\text{Vacancy})$, and $E(\text{M-Phosphorene})$ are the total energies of an isolated atom, the phosphorene layer with vacancy, and the doped atom-phosphorene system, respectively. The larger E_b represents the stronger binding of the atom to the phosphorene sheet.

3.2 Structural properties and binding energies

First, we computed the structural, energetic, electronic, magnetic properties for the monolayer phosphorene supercell doped with the single dopants. To check the stability of different dopants, we compare the binding energies,

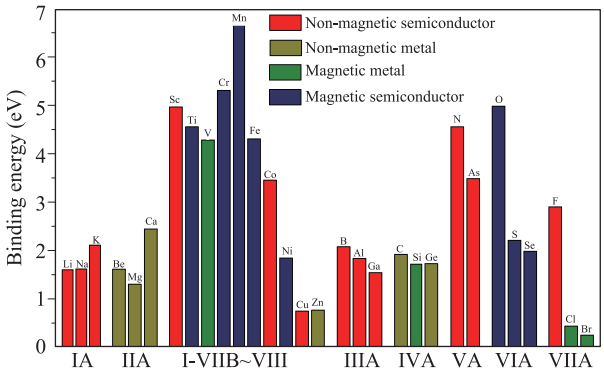

Fig. 2 Binding energies of phosphorene doped with 30 atoms from the periods two, three, and four. The doped systems are classified into four classes: non-magnetic semiconductors, non-magnetic metals, magnetic metals and magnetic semiconductors, which are distinguished with different colors.

as summarized in Fig. 2. The values of E_b for different dopants vary strongly from 0.25 to 6.65 eV. The binding energy decreases with the period for the IIIA, VA, VA, VIA, and VIIA groups. The values of E_b for 30 doped systems are larger than zero, which indicate that the substitutional doping of 30 atoms from the periods two, three, and four is energetically favorable.

According to our computed magnetic and electronic properties, we classify all the doped systems into four classes: non-magnetic semiconductors, non-magnetic metals, magnetic metals, and magnetic semiconductors, as shown in Fig. 2. The substitutional dopants from the VIA group induce the non-magnetic phosphorene to be a magnetic semiconductor, while the non-magnetic metal can be realized by the dopants from the IIA group. The phosphorene doped with the non-metal atoms of the IA, IIA, and VIA groups keeps a non-magnetic semiconductor. The situation becomes more complicated under the TM atoms doping. The origin and absence of magnetism for the doped systems will be discussed later.

Among the 30 doped phosphorene monolayers, we find the appearance of the magnetism for the O, S, Se, Cl, Br, Si, Ti, V, Fe, Ni, and Mn doping and the absence of the magnetism in other cases. The magnetic structures of nonmagnetic and magnetic atom doped phosphorene monolayers are investigated in detail. Table 1 lists the results of bond distances, binding energy, magnetic moment, and band gap of the single atom-doped phosphorene monolayers. We measure the interlayer and intralayer bond distances between the doping atom and the nearest phosphorus atoms which are denoted as $d_{M\text{-}P1}$ and $d_{M\text{-}P2} = d_{M\text{-}P3}$, respectively. Compared with the interlayer and intralayer P-P bond lengths of 2.27 Å and 2.22 Å in the pristine phosphorene, $d_{M\text{-}P1}$ changes more obvious than $d_{M\text{-}P2} = d_{M\text{-}P3}$. The difference between $d_{M\text{-}P1}$ or $d_{M\text{-}P2} = d_{M\text{-}P3}$ and the pristine bond length induced by the non-metal dopant atoms is larger than that induced by the TM atoms. In addition, the binding energy

Table 1 Structural, magnetic and electronic properties for O, S, Se, Cl, Br, Si, Ti, V, Fe, Ni, Cr and Mn doped in the 3×4 phosphorene supercell. $d_{M\text{-}P1}$ and $d_{M\text{-}P2} = d_{M\text{-}P3}$ are the distance between the dopant atom and the nearest neighboring phosphorus atom, respectively. Δd_1 and Δd_2 are the difference between the $d_{M\text{-}P1}$ or $d_{M\text{-}P2} = d_{M\text{-}P3}$ and the pristine P-P bonds, respectively. E_b and E_{bg} represent the binding energy of the corresponding dopant atom doped in phosphorene and graphene [40], respectively. μ_{iso} is the magnetic moment of the isolated atom in the unit of Bohr magneton (μ_B) and μ_{tot} is the total magnetic moment. E_{gap} is the energy gap of the system. For energy gap (E_{gap}), metallic and half-metallic structures are denoted as "m" and "hm", respectively.

Doped-atom	$d_{M\text{-}P1}$ (Å)	Δd_1 (Å)	$d_{M\text{-}P2} = d_{M\text{-}P3}$ (Å)	Δd_2 (Å)	E_b (eV)	$E_{bg}^{1)}$ (eV)	μ_{iso} (μ_B)	μ_{tot} (μ_B)	E_{gap} (eV)
O	3.15	0.88	1.71	−0.51	2.60	2.06	2.82	1.00	0.36
S	2.92	0.65	2.16	−0.06	2.85	–	2.85	1.00	0.16
Se	3.06	0.79	2.32	0.1	2.46	–	1.50	1.00	0.16
Cl	3.71	1.44	2.35	0.13	1.40	–	1.86	0.45	**m**
Br	3.80	1.53	2.48	0.26	1.22	–	2.40	0.28	**m**
Si	2.29	0.02	2.28	0.06	4.63	2.66	2.13	0.12	**m**
Ti	2.37	0.1	2.50	0.28	4.85	3.41	4.00	1.00	0.40
V	2.31	0.04	2.42	0.2	5.31	2.39	5.00	2.00	**hm**
Fe	2.18	−0.09	2.21	−0.01	4.28	2.70	3.00	1.00	0.16
Ni	2.17	−0.1	2.17	−0.05	4.44	4.09	2.00	1.00	0.16
Cr	2.25	−0.02	2.32	0.1	4.10	1.66	6.00	1.00	**hm**
Mn	2.31	0.04	2.38	0.16	2.92	1.78	5.00	3.97	0.12

[1)] Data from Ref. [40].

for the doping TM atoms is also larger than that of the non-metal doping atoms except for Si. We can conclude that the substitutional doping of TM atoms is more stable and induces smaller local structural distortion in the surface of the monolayer phosphorene than the nonmetal dopants.

3.3 Magnetic properties

Due to the sp^3 covalent bond between the neighboring P atoms, the pristine phosphorene is nonmagnetic. However, when doped with some non-magnetic nonmetal and magnetic TM atoms, monolayer phosphorene becomes magnetic, while some magnetic TM atoms doped systems have no magnetic state. For example, Sc-, Cu-, and Co-doped systems have no magnetic moment. Especially, the Co bulk structure is ferromagnetic and the isolated Co atom owns 3-μ_B magnetic moment, but the Co atom doped in the monolayer phosphorene causes the disappearance of magnetism. The configuration of Co valence shell is $3d^7 4s^2$. When the Co atom is embedded in the monolayer phosphorene, it is covalently bonded with the 3 neighboring P atoms by sharing its three valence electrons. Consequently, five valence electrons of each P atom are all paired and the remaining 6 electrons in the outmost valence shells of Co atom also form three electron pairs. Hence the phosphorene monolayer and Co atom are both nonmagnetic. Similarly, the pair and unpair of valence electrons can be used to explain the magnetism in the other cases of TM doping. Because of the tiny structural distortion, the magnetic moments of TM-doped phosphorene monolayers stem from the valence electrons of the TM $3d$ orbitals. Compared with the magnetic moments of the isolated TM atom, the magnetic moment of the TM-doped systems are suppressed in the range of 1.0–3.97 μ_B. For Ti, V, Fe, Ni, Cr, and Mn doped phosphorene monolayers, the systems are magnetic with the magnetic moment of 1.0 μ_B, 2.0 μ_B, 1.0 μ_B, 1.0 μ_B, 1.0 μ_B, and 3.97 μ_B.

3.4 Magnetization density

To investigate charge transfer and distribution between the substitutional doped atom and phosphorene monolayer, spin-polarized difference charge density of the magnetic structure is plotted in Fig. 3. The substitutional doped atoms are labeled with different colors. The local structures display that the upper and lower phosphorus atoms are displaced from their original positions after the nonmetal atom doping except for Si. Consequently, a noticeable local distortion around the dopants in phosphorene layer is observed and the local buckling feature of the phosphorene monolayer is destroyed, and this results in the change of bond length and electronic property.

The red color represents spin up density, while the green color represents spin down density. Spin density suggests that the magnetism originates mostly from the spin-up charge density of the TM atom and a little significant spin-down charge density is induced in the neighboring phosphorus atoms. In Cr, Fe, V, and Mn, the interaction between the TM atom and phosphorene seems a mixture

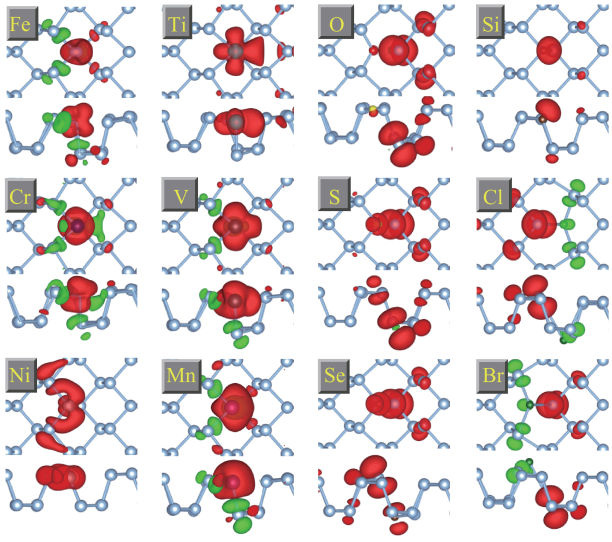

Fig. 3 Top and side view of the magnetization density for the nonmagnetic and magnetic atom doped phosphorene monolayers. The red color and green color have iso-values of 0.025 e/Å^3.

of covalent and ionic interaction. The spin polarization in each substitutional doped atom originates from different d orbitals. Especially for the nonmetal Si-doped system, the magnetic moment is entirely contributed from the spin-up charge density of Si atom. The O, S, and Se substitutional doping induces the spin polarization of the neighboring P atoms, and hence most spin-up charge density distributed around the neighboring P atoms is contributed to the magnetic moment. Different from the above cases, the magnetism of Cl- and Br-doped systems comes from both spin-down charge density located around the upper P atoms and spin-up charge density located around the lower P atoms instead of the dopants. This is mainly because of the strong structural distortion due to the substitutional doped atom.

3.5 Electronic properties

The substitutional doped phosphorene monolayers exhibit rich electronic properties. Figures 4(a)–(f) display the computed projected band structure and DOS of the single-atom O, S, Se, Ni, Ti, and V doped systems. Red lines imply the majority spin bands while black lines indicate the minority spin bands and the contribution of VBM and CBM from the different orbitals are distinguished with different colors. For the cases of O, S, and Se doping, the doped phosphorene monolayers become a spin semiconductor. The VBM and CBM are derived from the spin-up and spin-down states, respectively, while they are all contributed by the p_z orbital of the non-metal atom. The substitution of the three atoms gives rise to a magnetic moment of 1.0 μ_B.

The TM Ni-doped phosphorene turns the system into a narrow-band gap spin-semiconductor, and the spin-up and spin-down states form a 0.16 eV band gap. The system has a magnetic moment of 1.0 μ_B. The states at the Fermi surface mainly come from the d_{xy} state and the d_z^2 state of the TM Ni. For Ti-doped phosphorene monolayer, the system is also a spin-semiconductor with a narrow band gap of 0.40 eV and a total magnetic moment of 1.0 μ_B. But the state around the Fermi surface comes from the d_{yz}, d_{xz}, and d_x^2 orbitals. The up and down spin splitting of the d_x^2 orbital of Ti atom forms its CBM and VBM. The V-doped phosphorene has a half-metal feature and the total magnetic moment is 2.0 μ_B. The spin-up and spin-down orbitals overlap at the Fermi surface and they are contributed by the d_{xz} and d_{yz} orbitals of V atom, respectively. We also calculated the band structure of the V-doped phosphorene based on the HSE06, as plotted with the dashed lines in the Fig. 4(f). It is also supported that the V-doped system is half-metallic.

3.6 Discussion

Several experimental methods, such as pulsed laser deposition, intercalation, chemical modification, low-energy ion implantation and defect-assisted doping by electron beam irradiation, have proved possible to introduce dopants into nanosheet materials [41, 42]. For instance, it has been reported experimentally that pulsed laser deposition can be used to dope graphene with single TM atoms, such as Pt, Co, and In [28]. As listed in the Table 1, our computed binding energy for the O, Si, Ti, V, Fe, Ni, Cr, and Mn doping in the monolayer phosphorene is larger than that of the corresponding dopant in graphene, which indicates that the experimental realization of the substitution of the impurities in monolayer phosphorene is possible and stable. We expect that similar experimental method can be applied to monolayer phosphorene to realize single atom doping. Thus, potential applications in spintronic devices and dilute magnetic semiconductors, and the possibility of half metallicity induced by the substitutional doping in the phosphorene sheets will be explored and realized.

4 Conclusion

In conclusion, we have explored structural, magnetic, and electronic properties of 30 metal- and nonmetal-doped phosphorene monolayers by using density functional theory computations. The magnetic moment of the TM-doped system is suppressed from its bulk value, which can be explained with the pair and unpair of the 3d valence electrons of TM. The nonmetal O, S, Se, Si, Br, and Cl doping induces strong lattice distortion, which modulates the magnetism and electronic property of the doped systems. Our computations demonstrated that 2D diluted magnetic semiconducting and spin semiconducting systems can be realized by the dopants in the monolayer

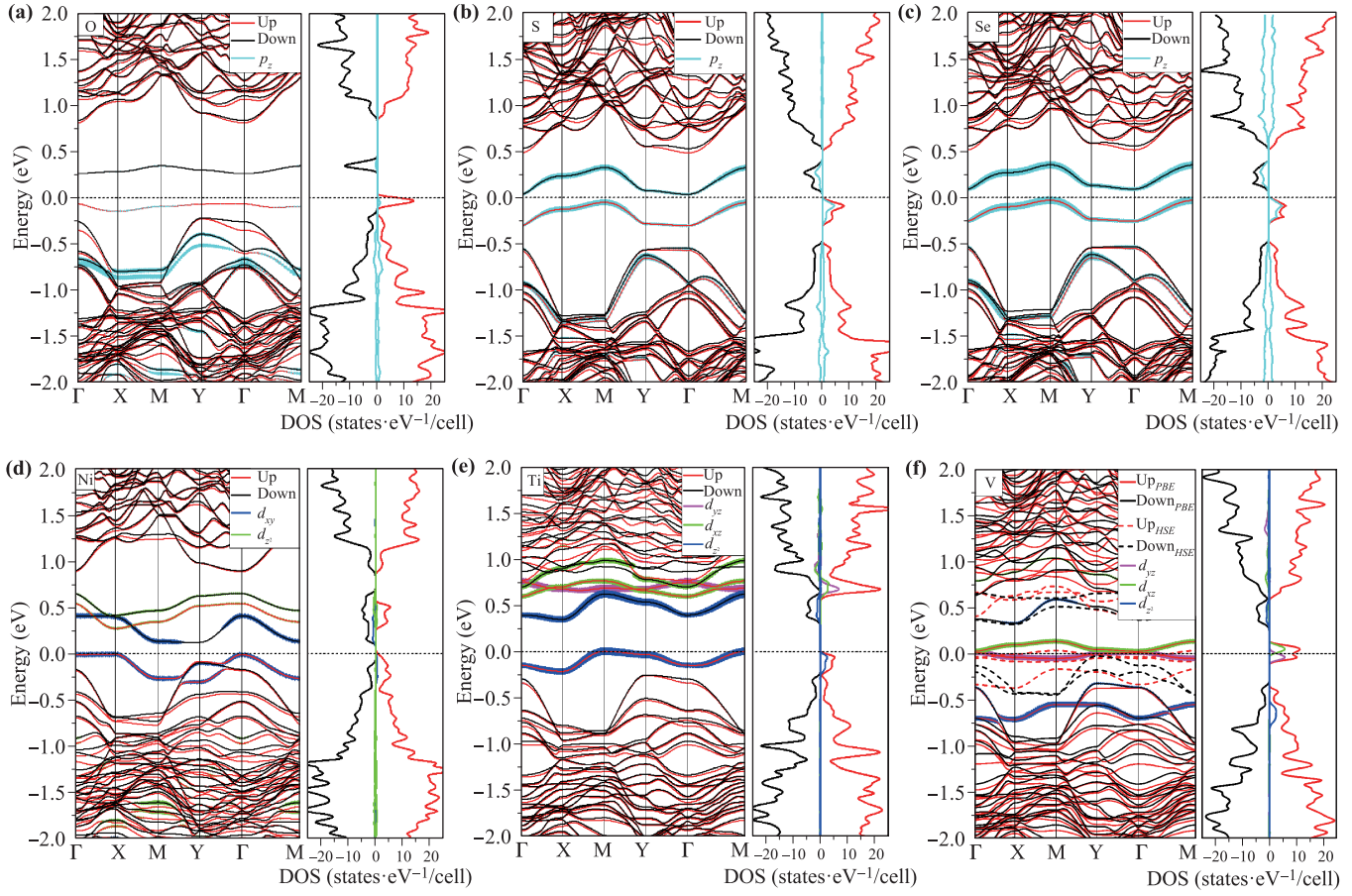

Fig. 4 Spin polarized projected electronic band structure (left) and DOS (right) for the doped monolayer phosphorene. **(a)** O-doped system. **(b)** S-doped system. **(c)** Se-doped system. **(d)** Ni-doped system. **(e)** Ti-doped system. **(f)** V-doped system. The Fermi energy is shifted to zero energy as indicated by the horizontal dashed black line.

phosphorene; particularly it is promising for doping monolayer phosphorene by O, S, Se, Ti, V, and Ni. The value of E_b for these doping is larger than that of the corresponding dopants in the graphene, which indicates that the doped systems can be realized in experiments.

Acknowledgements This research was supported by the National Key Research and Development Program of China under Grant No. 2018YFB0703900 and the National Natural Science Foundation of China under Grant No. 11704322.

References

1. A. K. Geim and K. S. Novoselov, The rise of graphene, *Nat. Mater.* 6(3), 183 (2007)
2. A. H. Castro Neto, F. Guinea, N. M. R. Peres, K. S. Novoselov, and A. K. Geim, The electronic properties of graphene, *Rev. Mod. Phys.* 81(1), 109 (2009)
3. F. Schwierz, Graphene transistors, *Nat. Nanotechnol.* 5(7), 487 (2010)
4. Y. Wu, Y. M. Lin, A. A. Bol, K. A. Jenkins, F. Xia, D. B. Farmer, Y. Zhu, and P. Avouris, High-frequency, scaled graphene transistors on diamond-like carbon, *Nature* 472(7341), 74 (2011)
5. H. Liu, A. T. Neal, Z. Zhu, Z. Luo, X. Xu, D. Tománek, and P. D. Ye, Phosphorene: An unexplored 2D semiconductor with a high hole mobility, *ACS Nano* 8(4), 4033 (2014)
6. K. F. Mak, C. Lee, J. Hone, J. Shan, and T. F. Heinz, Atomically thin MoS_2: A new direct-gap semiconductor, *Phys. Rev. Lett.* 105(13), 136805 (2010)
7. A. Splendiani, L. Sun, Y. B. Zhang, T. S. Li, J. Kim, C. Y. Chim, G. Galli, and F. Wang, Emerging photoluminescence in monolayer MoS_2, *Nano Lett.* 10(4), 1271 (2010)
8. P. M. Bridgman, Two new modifications of phosphorus, *J. Am. Chem. Soc.* 36(7), 1344 (1914)
9. T. Nishii, Y. Maruyama, T. Inabe, and I. Shirotani, Synthesis and characterization of black phosphorus intercalation compounds, *Synth. Met.* 18(1–3), 559 (1987)
10. L. Li, Y. Yu, G. J. Ye, Q. Ge, X. Ou, H. Wu, D. Feng, X. H. Chen, and Y. Zhang, Black phosphorus field-effect transistors, *Nat. Nanotechnol.* 9(5), 372 (2014)
11. E. S. Reich, Phosphorene excites materials scientists, *Nature* 506(7486), 19 (2014)

12. L. Shulenburger, A. D. Baczewski, Z. Zhu, J. Guan, and D. Tománek, The nature of the interlayer interaction in bulk and few-layer phosphorus, *Nano Lett.* 15(12), 8170 (2015)
13. T. Low, R. Rold'an, H. Wang, F. N. Xia, P. Avouris, L. M. Moreno, and F. Guinea, Plasmons and screening in monolayer and multilayer black phosphorus, *Phys. Rev. Lett.* 113(10), 106802 (2014)
14. A. S. Rodin, A. Carvalho, and A. H. Castro Neto, Strain-induced gap modification in black phosphorus, *Phys. Rev. Lett.* 112(17), 176801 (2014)
15. X. Ling, H. Wang, S. Huang, F. Xia, and M. S. Dresselhaus, The renaissance of black phosphorus, *Proc. Natl. Acad. Sci. USA* 112(15), 4523 (2015)
16. J. Qiao, X. Kong, Z. Hu, F. Yang, and W. Ji, High-mobility transport anisotropy and linear dichroism in few-layer black phosphorus, *Nat. Commun.* 5(1), 4475 (2014)
17. F. Xia, H. Wang, and Y. Jia, Rediscovering black phosphorus as an anisotropic layered material for optoelectronics and electronics, *Nat. Commun.* 5(1), 4458 (2014)
18. R. Schuster, J. Trinckauf, C. Habenicht, M. Knupfer, and B. Büchner, Anisotropic particle-hole excitations in black phosphorus, *Phys. Rev. Lett.* 115(2), 026404 (2015)
19. J. Kim, S. S. Baik, S. H. Ryu, Y. Sohn, S. Park, B. G. Park, J. Denlinger, Y. Yi, H. J. Choi, and K. S. Kim, Observation of tunable band gap and anisotropic Dirac semimetal state in black phosphorus, *Science* 349(6249), 723 (2015)
20. P. K. Li and I. Appelbaum, Electrons and holes in phosphorene, *Phys. Rev. B* 90(11), 115439 (2014)
21. J. W. Jiang and H. S. Park, Negative Poisson's ratio in single-layer black phosphorus, *Nat. Commun.* 5(1), 4727 (2014)
22. K. Sato, L. Bergqvist, J. Kudrnovský, P. H. Dederichs, O. Eriksson, I. Turek, B. Sanyal, G. Bouzerar, H. Katayama-Yoshida, V. A. Dinh, T. Fukushima, H. Kizaki, and R. Zeller, First-principles theory of dilute magnetic semiconductors, *Rev. Mod. Phys.* 82(2), 1633 (2010)
23. Z. F. Wang, S. Jin, and F. Liu, Spatially separated spin carriers in spin-semiconducting graphene nanoribbons, *Phys. Rev. Lett.* 111(9), 096803 (2013)
24. Y. C. Zhao and J. Ni, Spin-semiconducting properties in silicene nanoribbons, *Phys. Chem. Chem. Phys.* 16(29), 15477 (2014)
25. M. I. Katsnelson, V. Yu. Irkhin, L. Chioncel, A. I. Lichtenstein, and R. A. de Groot, Half-metallic ferromagnets: From band structure to many-body effects, *Rev. Mod. Phys.* 80(2), 315 (2008)
26. Y. Son, M. L. Cohen, and S. G. Louie, Half-metallic graphene nanoribbons, *Nature* 444(7117), 347 (2006)
27. D. D. Awschalom and M. E. Flatte, Challenges for semiconductor spintronics, *Nat. Phys.* 3(3), 153 (2007)
28. H. T. Wang, Q. X. Wang, Y. C. Cheng, K. Li, Y. B. Yao, Q. Zhang, C. Z. Dong, P. Wang, U. Schwingenschlögl, W. Yang, and X. X. Zhang, Doping monolayer graphene with single atom substitutions, *Nano Lett.* 12(1), 141 (2012)
29. A. V. Krasheninnikov, P. O. Lehtinen, A. S. Foster, P. Pyykkö, and R. M. Nieminen, Embedding transition-metal atoms in graphene: Structure, bonding, and magnetism, *Phys. Rev. Lett.* 102(12), 126807 (2009)
30. R. Wang, X. G. Ren, Z. Yan, L. J. Jiang, W. E. I. Sha, and C. G. Shan, Graphene based functional devices: A short review, *Front. Phys.* 14(1), 13603 (2019)
31. Z. N. Ma, J. B. Zhuang, X. Zhang, and Z. Zhou, SiP monolayers: New 2D structures of group IV–V compounds for visible-light photohydrolytic catalysts, *Front. Phys.* 13(3), 138104 (2018)
32. F. M. Xu, Z. Z. Yu, Z. R. Gong, and H. Jin, First-principles study on the electronic and transport properties of periodically nitrogen-doped graphene and carbon nanotube superlattices, *Front. Phys.* 12(4), 127306 (2017)
33. G. Kresse and J. Hafner, *Ab initio* molecular dynamics for liquid metals, *Phys. Rev. B* 47(1), 558 (1993)
34. G. Kresse and D. Joubert, From ultrasoft pseudopotentials to the projector augmented-wave method, *Phys. Rev. B* 59(3), 1758 (1999)
35. J. P. Perdew, K. Burke, and M. Ernzerhof, Generalized gradient approximation made simple, *Phys. Rev. Lett.* 77(18), 3865 (1996)
36. H. J. Monkhorst and J. D. Pack, Special points for Brillouin-zone integrations, *Phys. Rev. B* 13(12), 5188 (1976)
37. A. Brown and S. Rundqvist, Refinement of the crystal structure of black phosphorus, *Acta Crystallogr.* 19(4), 684 (1965)
38. X. H. Peng, Q. Wei, and A. Copple, Strain-engineered direct-indirect band gap transition and its mechanism in two-dimensional phosphorene, *Phys. Rev. B* 90(8), 085402 (2014)
39. S. Das, W. Zhang, M. Demarteau, A. Hoffmann, M. Dubey, and A. K. Roelofs, Tunable transport gap in phosphorene, *Nano Lett.* 14(10), 5733 (2014)
40. K. T. Chan, J. Neaton, and M. L. Cohen, First-principles study of metal adatom adsorption on graphene, *Phys. Rev. B* 77(23), 235430 (2008)
41. T. T. Tung, F. Alotaibi, M. J. Nine, R. Silva, D. N. H. Tran, I. Janowska, and D. Losic, Engineering of highly conductive and ultra-thin nitrogen-doped graphene films by combined methods of microwave irradiation, ultrasonic spraying and thermal annealing, *Chem. Eng. J.* 338, 764 (2018)
42. D. Mombrú, R. Faccio, and A. W. Mombru, Possible causes for rippling in a multivacancy graphene system, *Int. J. Quantum Chem.* 118(7), e25529 (2018)